Reducing the RCS of a MIMO Antenna Using an Angularly Stable FSS

Sreenath Reddy Thummaluru and Raghvendra Kumar Chaudhary

Department of Electronics Engineering
Indian Institute of Technology
(Indian School of Mines)
Dhanbad, India
E-mails: sreenath966@gmail.com; raghvendra.chaudhary@gmail.com

Abstract

A systematic design procedure for reducing the radar cross section (RCS) of a multiple-input multiple-output (MIMO) antenna is presented in this paper. The RCS reduction was achieved at 11.3 GHz, which was out-of-band compared to the antenna's working frequency of 2.18 GHz. The design flow started with developing an isolation-enhancement network for the MIMO antenna that did not disturb the RCS reduction process. An incident- and polarization-angle-insensitive frequency-selective surface (FSS) was next designed. The conventional ground plane of the MIMO antenna was replaced by an FSS array. The designed FSS was introduced in such a way that the antenna's characteristics and isolation among the antenna ports were preserved by achieving the RCS reduction of an antenna at the bandpass frequency of the FSS. The proposed FSS was angularly stable, and hence an almost constant RCS reduction was found for most of the incident angles. The final proposed low-RCS MIMO antenna was fabricated and measured to validate the simulation results.

1. Introduction

To meet the ever-growing demands of high data rates and excellent data transmission in wireless communication, multiple-input multiple-output (MIMO) technology was introduced. Single-input single-output (SISO) technology is being replaced by MIMO technology on all platforms. The Defense Advanced Research Projects Agency (DARPA) recognized the significance of using MIMO technology in defense applications for the sake of increasing the war fighter's capabilities [1]. The Wireless Networking and Communications Group (WNCG) talks about the usefulness of MIMO technology in military applications [2].

In the defense and military environment, some applications require low RCS materials. By using antennas in defense applications, the RCS will be drastically increased because the antennas are backed by a PEC ground plane. To address this problem, researchers have proposed many antenna RCS reduction techniques. These include using RCS reduction techniques based on a radar-absorbing material (RAM) [3, 4], an antenna coating [5], a frequency-selective surface (FSS) [6, 7], a metasurface [8, 9], and an artificial magnetic conductor (AMC) [10]. For applications where size matters, FSS- and metasurface-based RCS reduction techniques seem to be the most efficient, because they do not involve any extra circuitry, unlike other techniques. However, if the FSS-based RCS reduction technique is to be applied to MIMO antennas, the isolation among the antenna ports should first be addressed. The involvement of an FSS in a MIMO antenna disturbs the surface-current distribution, which in turn affects the isolation between the antenna elements [11]. A compatible isolation-enhancement network is thus needed for MIMO antennas before beginning the RCS-reduction process.

In the literature, there are various isolation-enhancement techniques for MIMO antennas. They can be divided into five major categories. These are the use of defected ground structures (DGS) [12, 13], parasitic elements [14, 15], neutralization lines [16, 17], decoupling networks [18, 19], and metamaterials [20, 21]. Among these, isolation techniques based on defected ground structures, neutralization lines, and parasitic elements disturb the surface current distribution between antenna elements to enhance the isolation between the elements. Because the involvement of an FSS in the ground plane of a MIMO antenna for RCS reduction also disturbs the surface current, those three isolation techniques are not suitable for the RCS-reduction process. A decoupling network in a MIMO antenna provides isolation between the antenna ports by not letting the surface waves propagate from one antenna element to other elements. Metamaterials utilize their bandgap nature to provide isolation among the antenna elements of a MIMO antenna. Both these isolation techniques are compatible with use in the RCS-reduction process of MIMO antenna systems.

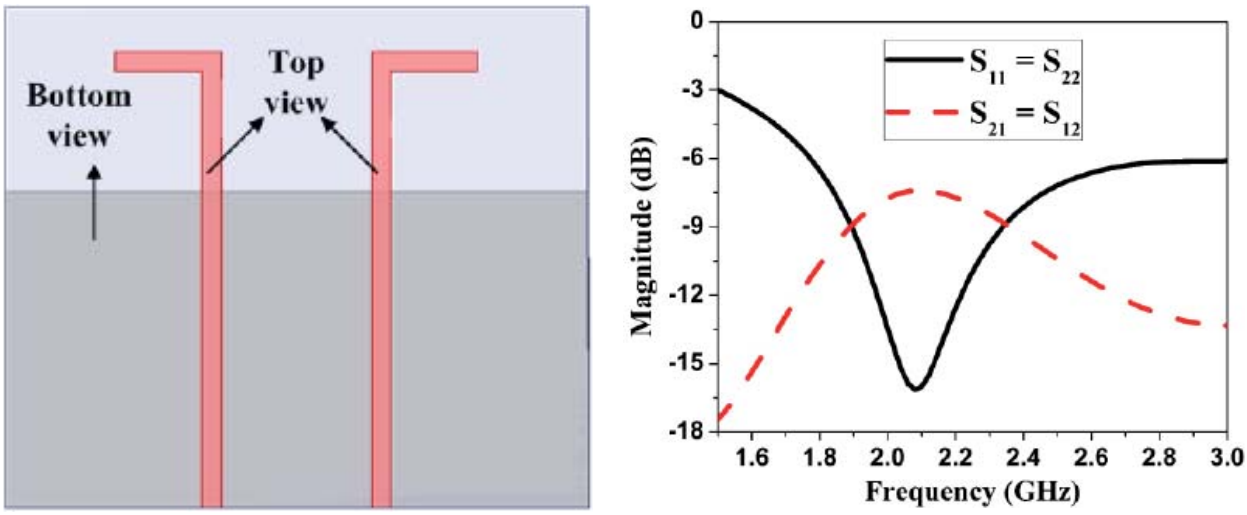

Figure 1. A simple two-port antenna: (a) the design, and its (b) *S* parameters (simulated).

In this work, we developed a filter-based decoupling network to enhance the isolation in MIMO antennas, making it suitable for the RCS-reduction process. The novelty of this paper is that the proposed isolation-enhancement circuit and RCS-reduction circuit are independent. Controlling one circuit will not affect the other. Even though FSS-based RCS-reduction techniques have been proposed in the literature, they are not insensitive to the angle of incidence. In order to provide constant RCS reduction for all the incident angles, an angularly stable FSS was developed.

2. A MIMO Antenna Design Having a Filter-Based Decoupling Network

For all the designs that are provided in this paper, the base substrate was FR4 with a thickness of 1.6 mm.

The design process started with the two-element antenna shown in Figure 1a. The two monopole antennas are shown in Figure 1a: they were closely spaced, without any decoupling network. The isolation was hence very poor in between them at the antenna's resonant frequency of 2.08 GHz, shown in Figure 1b. To enhance the isolation between the antenna elements, a decoupling network was designed at 2.08 GHz, as shown in Figure 2a. From its *S* parameters, as shown in Figure 2b, a band-stop property could be identified at 2.08 GHz.

In the next step, this band-stop filter was inserted in between the antenna elements of a two-port MIMO antenna, shown in Figure 3a. By directly inserting the decoupling network, isolation was achieved, but with the resonant frequency of the antenna shifted away from 2.08 GHz as shown in Figure 3b. To achieve both resonance and isolation at the same frequency, i.e., at 2.08 GHz, a matching network in the form of stubs was therefore used. The final proposed MIMO antenna, along with matching and decoupling networks, is shown in Figure 4a. The dimensions of the elements in Figure 4a were $a = 58$, $b = 50$, $c = 41.9$, $d = 19.5$, $e = 18.5$, $f = 15$, $g = 12.7$, $h = 12$, $i = 10.6$,

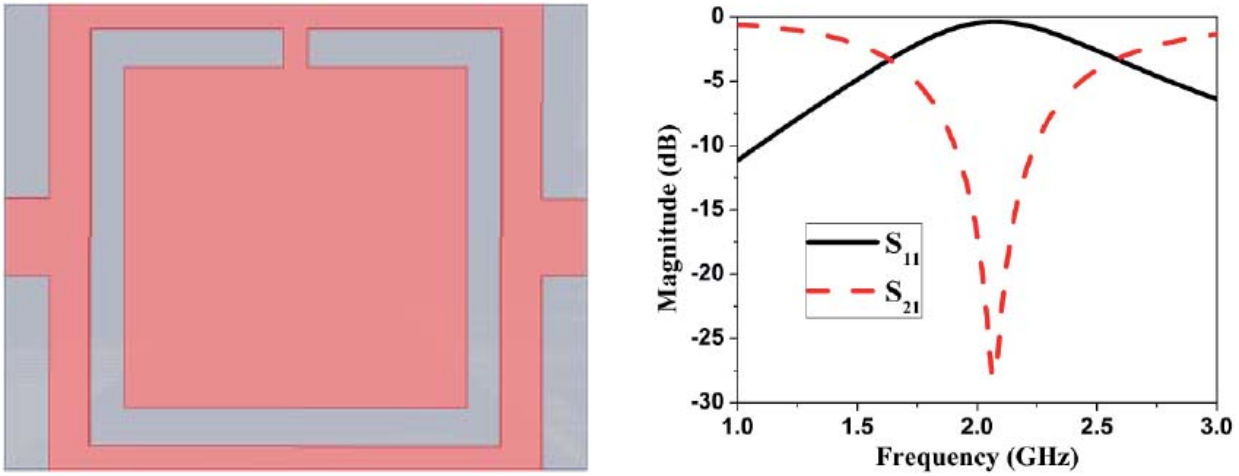

Figure 2. The decoupling network (band-stop filter): (a) the design, and its (b) *S* parameters (simulated).

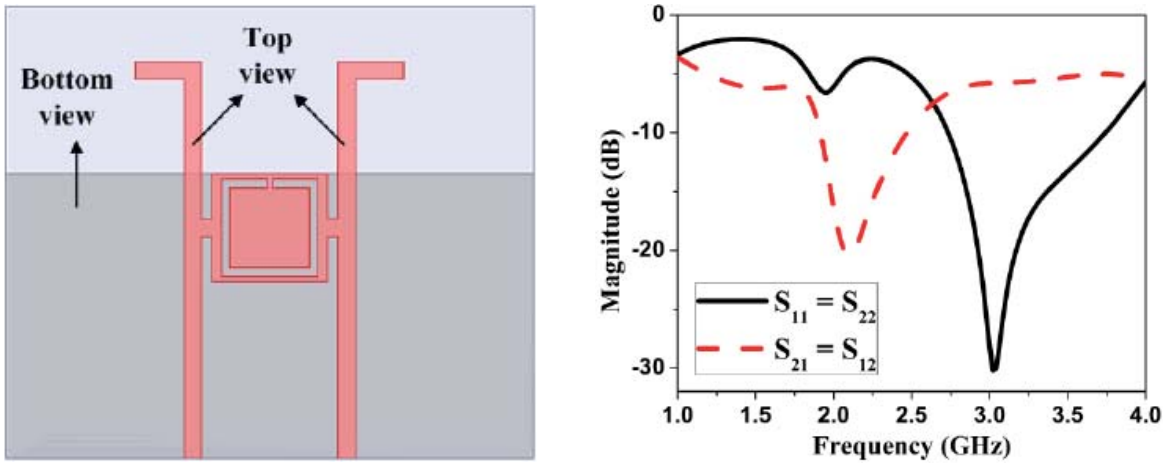

Figure 3. The two-port antenna with decoupling network: (a) design, and its (b) *S* parameters (simulated).

$j = 8.85$, $k = 7.25$, $l = 4.1$, $m = 3$, $n = 1.9$, and $o = 1$ (all in mm). From its *S*-parameter plot, shown in Figure 4b, one could observe that more than 16 dB isolation was achieved in the antenna's working band.

To get a clear idea of how the isolation was enhanced by using the decoupling network, the surface-current distribution is shown on the MIMO antenna at 1 GHz and 2.08 GHz in Figure 5. Both of the plots in Figure 5 were obtained by exciting only one port while terminating the other port with a matching impedance. From Figure 4b, at 2.08 GHz, the isolation was very high as compared to the isolation at 1 GHz. The same could be observed by looking at Figure 5. In Figure 5a, the surface current from the excitation port was not flowing towards the terminated port. In contrast, in Figure 5b, a maximum surface current was flowing. This was the reason for less isolation at 1 GHz, as shown in Figure 4b.

The fabricated MIMO antenna's top and bottom portions are shown in Figures 6a and 6b, respectively. The simulated *S* parameters were validated by measuring them, as shown in Figure 7a. Good agreement was found between measured and simulated results. The proposed MIMO antenna exhibited around 2 dBi peak gain and more than 70% radiation efficiency at the antenna's working frequency, as shown in Figure 7b. The peak gain in Figure 7b was a measured result, whereas the radiation efficiency was a simulated result. In both the *xz* and *yz* planes, the measured two-dimensional radiation patterns along with the simulated patterns are shown in Figure 8. These radiation patterns were calculated at the antenna's resonant frequency of 2.08 GHz. The given radiation patterns were obtained by exciting only one antenna element. However, because both of the antenna elements were symmetrical, similar kinds of radiation patterns with a 180° phase shift could be obtained by exciting the other antenna element. The envelope correlation coefficient (ECC) and capacity loss are important parameters for estimating MIMO performance. In this paper, both of these parameters were measured and are shown in Figure 9. In the antenna's working band, both of these MIMO parameters were within the allowable limits [22, 23]. It hence could be said that the proposed two-port antenna was a suitable candidate for MIMO applications.

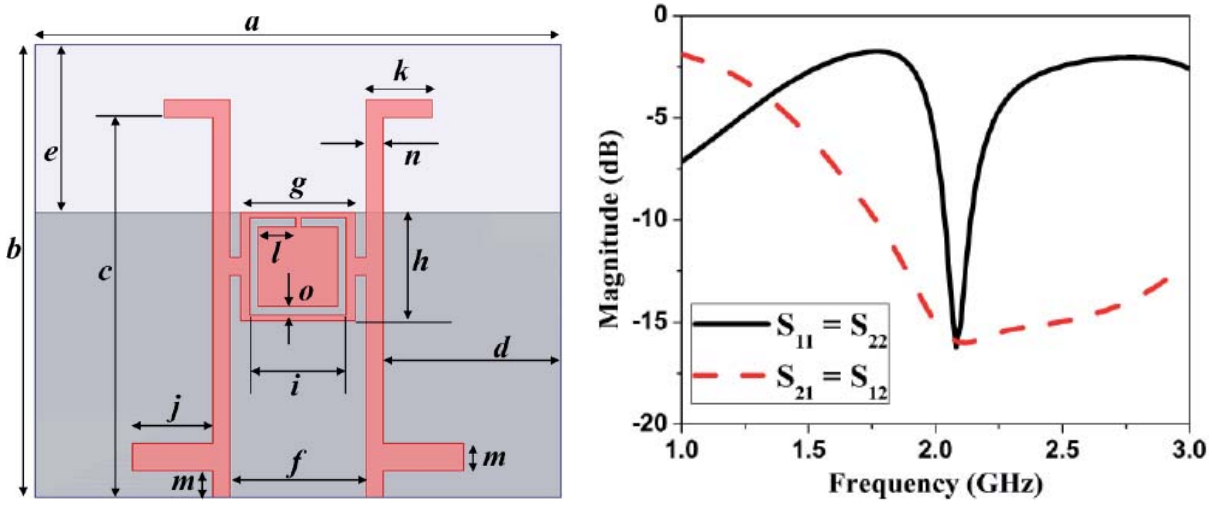

Figure 4. The proposed two-port MIMO antenna: (a) the design, and its (b) *S* parameters (simulated).

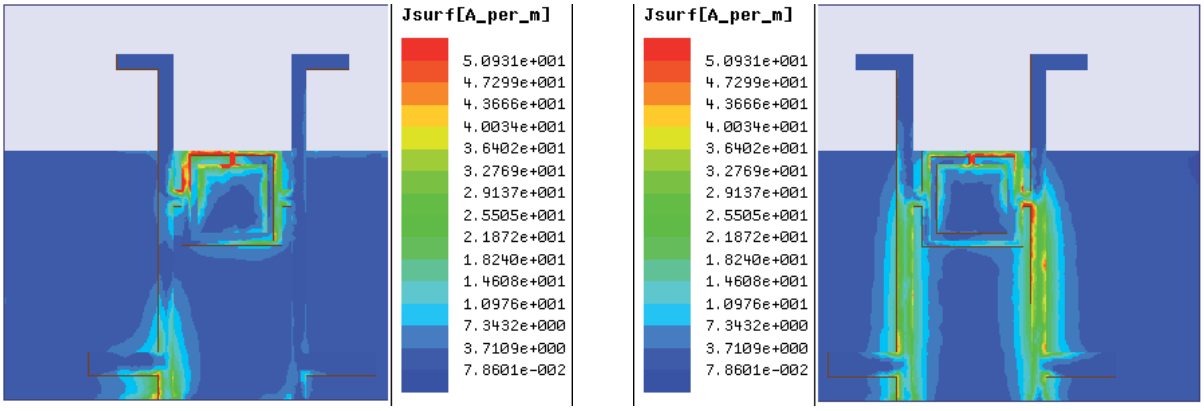

Figure 5. The surface-current distribution on the MIMO antenna at (a) 2.08 GHz and (b) 1 GHz.

3. Reducing the RCS of the MIMO Antenna

In the previous section, the design of a MIMO antenna using a filter-based decoupling network was shown. The procedure for reducing the RCS of the designed antenna is presented in this section. The first step in an RCS-reduction process is designing an FSS at a frequency where the RCS reduction of the MIMO antenna is needed. Here, two FSS designs are presented to explain the importance of an angularly stable FSS in making the RCS reduction incident-angle insensitive. The first FSS is denoted as FSS_1, and

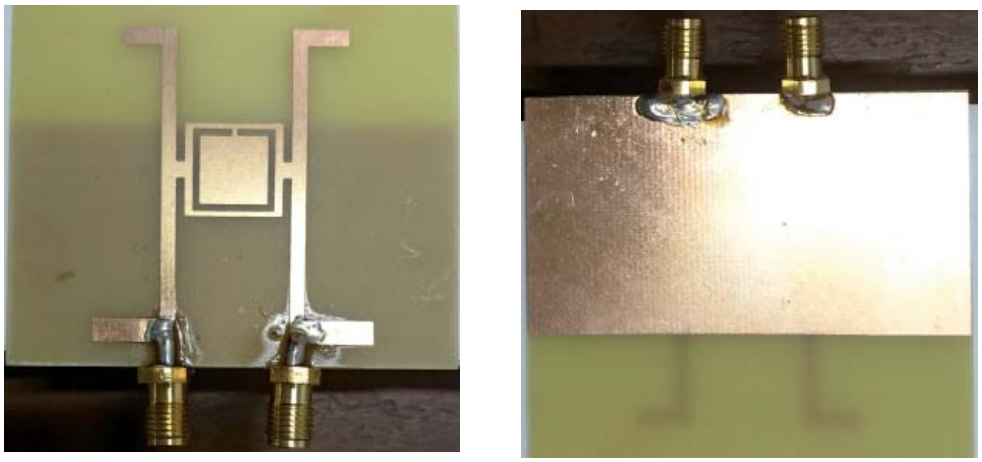

Figure 6. The (a) top and (b) bottom views of the fabricated proposed MIMO antenna.

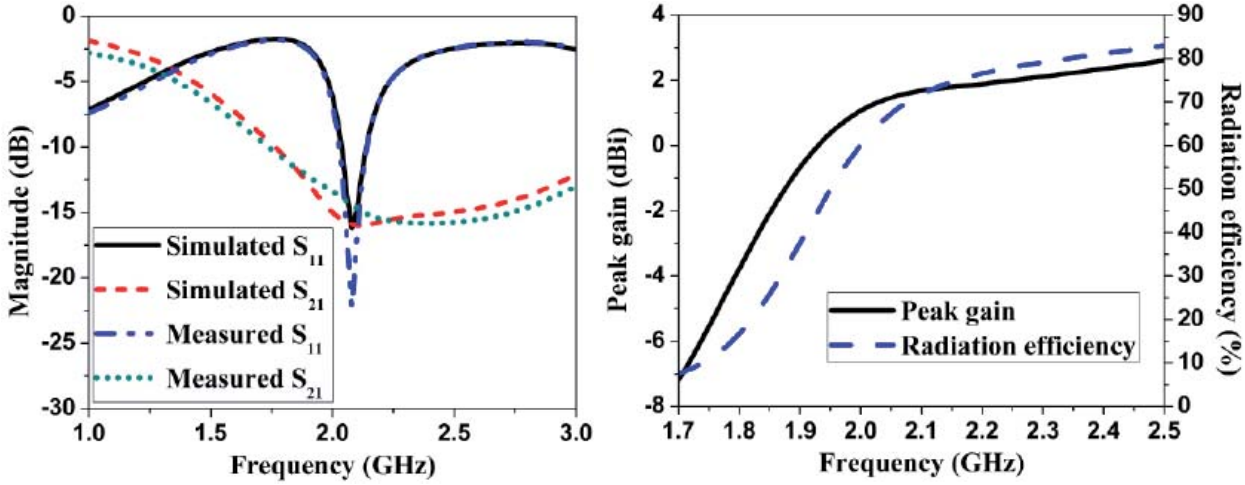

Figure 7. (a) A comparison of simulated and measured *S* parameters, and (b) the peak gain (measured) and radiation efficiency (simulated) of the antenna.

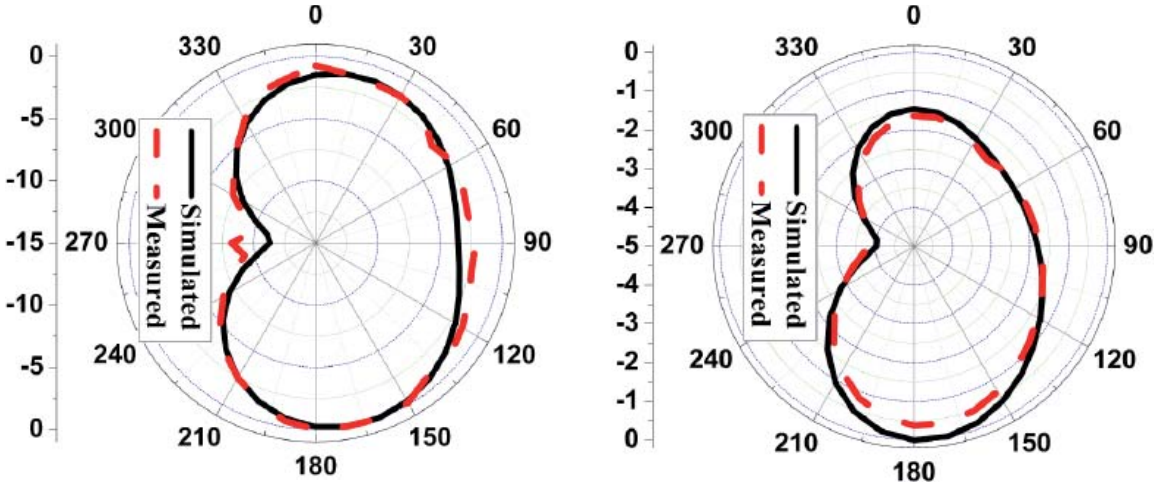

Figure 8. MIMO antenna radiation patterns at 2.08 GHz in (a) the *xz* plane and (b) the *yz* plane.

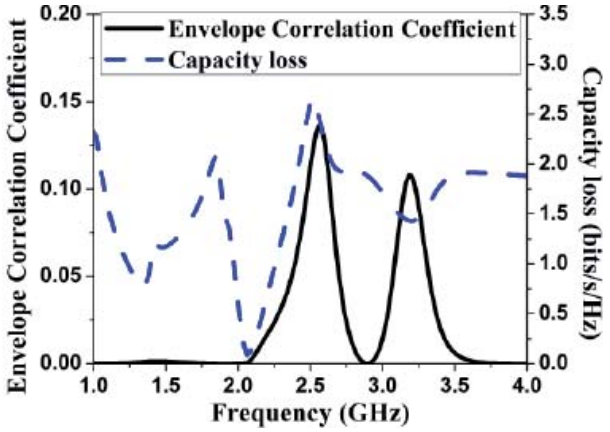

Figure 9. The measured MIMO parameters (ECC and capacity loss).

the second FSS is identified as FSS_2. The design of a single unit cell of FSS_1 is shown in Figure 10a, and a plot of its *S* parameters is shown in Figure 10b. FSS_1 exhibited bandpass characteristics at 10.6 GHz, with reflection coefficient (R_C) and transmission coefficient (T_C) values of around −15 dB and 0 dB, respectively. FSS_1 was arranged in the ground plane of the MIMO antenna in such a way that the upper conductive microstrip line part was backed by a PEC [7], as shown in Figure 11a. With this arrangement, not only radiating part of the antenna but also the decoupling network did not get disturbed. Reducing the RCS was hence possible without disturbing both the antenna characteristics and the isolation between the antenna elements. If a different isolation-enhancement network other than the decoupling network was used, then it would not have been easy to maintain high isolation between the antenna elements by arranging the FSS array in a ground plane. From Figures 4b and 11b, it was observed that the *S* parameters remained same for the MIMO antenna when backed by either a PEC or FSS_1.

Since FSS_1 acted like a transmitter of an EM wave at 10.6 GHz, an RCS reduction of more than 15 dB was achieved at the same frequency by the MIMO antenna backed by FSS_1 as compared to the MIMO antenna backed by the PEC, as shown in Figure 12b. Since FSS_1 had four-fold symmetry, it remained polarization-angle insensitive.

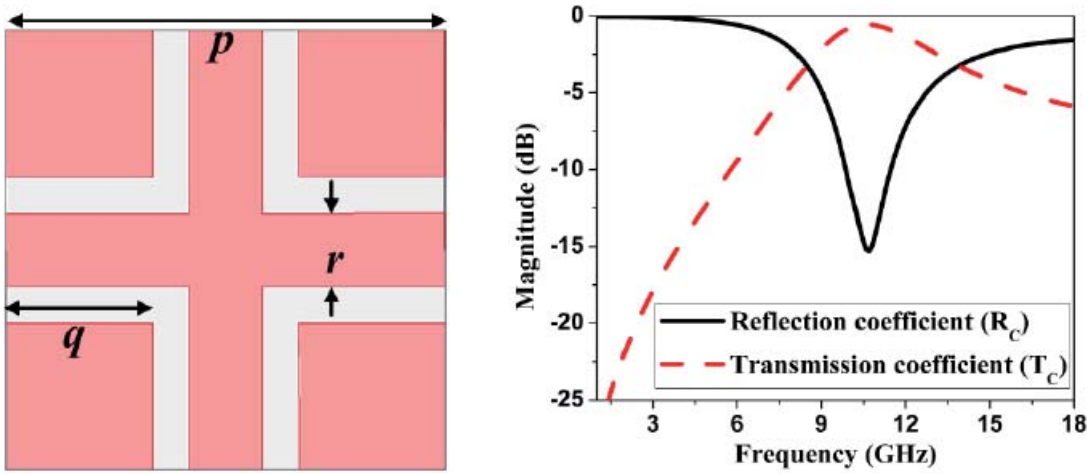

Figure 10. (a) The FSS_1 unit cell and its (b) reflection and transmission properties (simulated) ($p = 6$ mm, $q = 2$ mm, $r = 1$ mm).

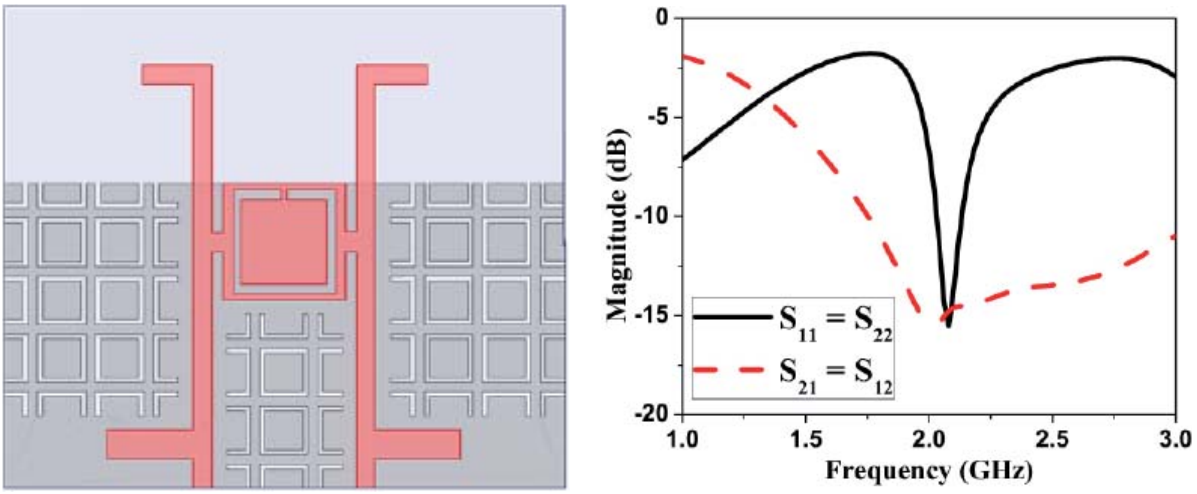

Figure 11. (a) The design of the MIMO antenna with an array based on FSS_1 as its background, and its (b) simulated *S* parameters.

However, by increasing the angle of incidence, reflections from FSS_1 drastically increased, as shown in Figure 12a. For incident angles of more than 60°, FSS_1 almost lost its bandpass property at 10.6 GHz. From Figure 12b, it could be observed that the amount of RCS reduction also drastically decreased for higher incidence angles. From Figures 12a and 12b it could thus be concluded that the reflections from FSS_1 played a prominent role in finding the RCS of the proposed design.

To understand this theoretically, an explanation using ray theory was given. The FSS reflection coefficient under normal incidence can be written as

$$\Gamma_{FSS} = \frac{\eta_{FSS} - \eta_0}{\eta_{FSS} + \eta_0}, \quad (1)$$

$$\eta_{FSS} = \eta_0 \sqrt{\frac{\mu_{FSS}}{\varepsilon_{FSS}}},$$

where μ_{FSS}, ε_{FSS}, and η_{FSS} are respectively the permeability, permittivity, and intrinsic impedance of the FSS. Γ_{FSS} is the reflection coefficient of the FSS under normal incidence. η_0 is the free-space intrinsic impedance.

When the permittivity and permeability of the FSS in Equation (1) become equal to the free-space intrinsic impedance, reflections from the FSS become very small, and a reduction in the RCS is possible for the MIMO antenna with the FSS as compared to a MIMO antenna with a PEC. However, it is not that simple to analyze the reduction in RCS when the antenna is under oblique incidence. The reflection coefficient at oblique incidence for TE polarization can be written as

$$\Gamma_{OTE} = \frac{\eta_{FSS}\cos\theta_i - \eta_0\cos\theta_t}{\eta_{FSS}\cos\theta_i + \eta_0\cos\theta_t}, \quad (2)$$

where Γ_0 is the oblique-incidence reflection coefficient,

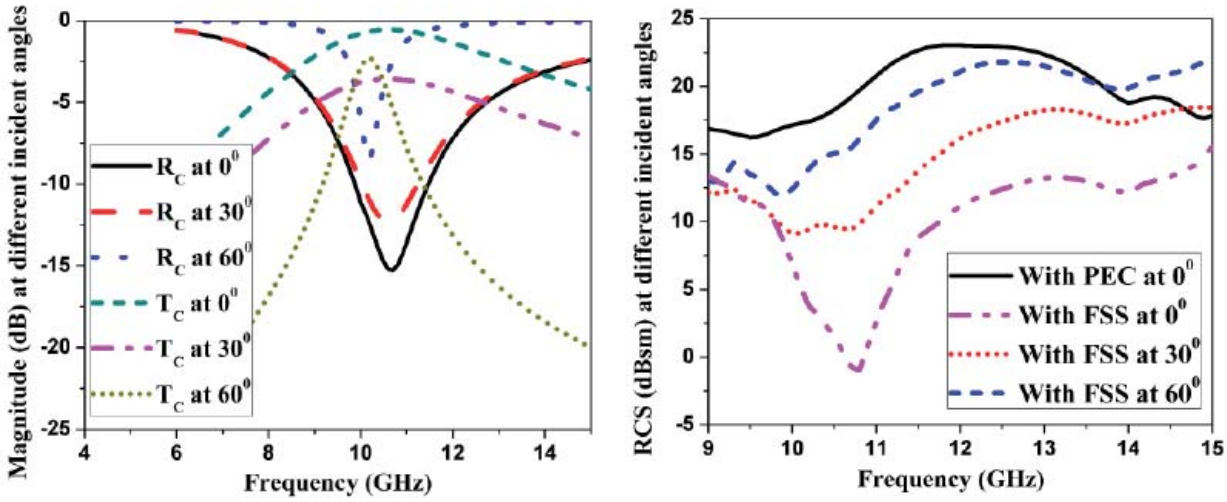

Figure 12. (a) The simulated T_C and R_C for FSS_1 at oblique incidence, and (b) the simulated RCS of the MIMO antenna with FSS_1 at oblique incidence.

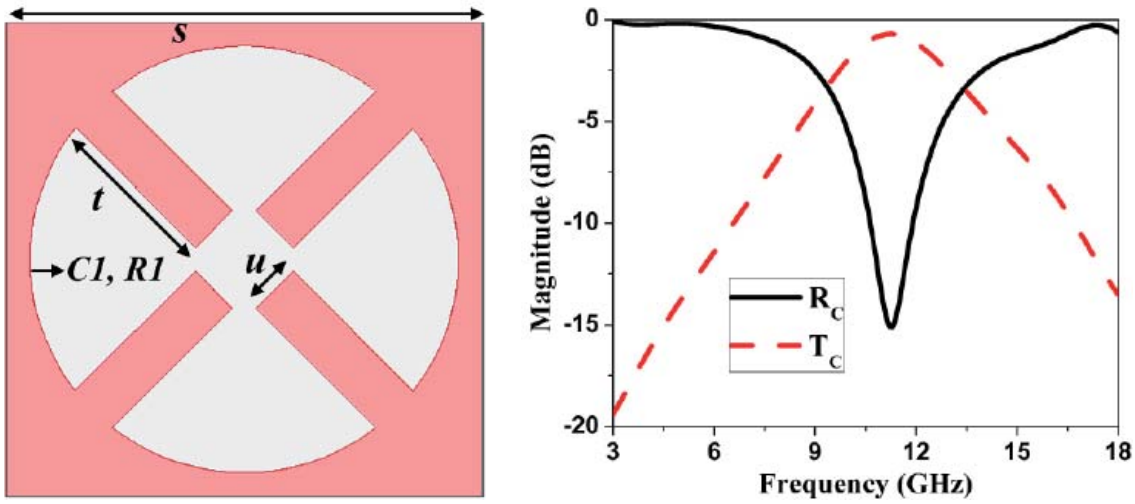

Figure 13. (a) The unit cell of FSS_2, and its (b) simulated reflection and transmission ($s = 6$ **mm,** $t = 2.136$ **mm,** $u = 0.659$ **mm,** $C1 = (3$ **mm**, 3 **mm) ,** $R1 = 2.7$ **mm).**

and θ_i and θ_t are the angles of incidence and transmission. By using Snell's law, the relationship between the intrinsic impedance of free space and the impedance of the FSS can be written as

$$\frac{\eta_0}{\eta_{FSS}} = \frac{\sin\theta_t}{\sin\theta_i} . \tag{3}$$

By solving Equations (3) and (2), the minimum reflection condition can be obtained:

$$MR_{cri_{TE}} = \mu_{FSS}\varepsilon_{FSS} - \varepsilon_{FSS}^2 \sin^2\theta_i - \mu_{FSS}^2 \cos^2\theta_i = 0 \tag{4}$$

For the TM-polarized wave, the reflection coefficient under oblique incidence can be written as

$$\Gamma_{OTM} = \frac{\eta_{FSS}\cos\theta_t - \eta_0\cos\theta_i}{\eta_{FSS}\cos\theta_t + \eta_0\cos\theta_i} . \tag{5}$$

By following a similar procedure, the minimum-reflection condition for TM polarization was calculated:

$$MR_{cri_{TM}} = \mu_{FSS} - \varepsilon_{FSS}\sin^2\theta_i - \mu_{FSS}\varepsilon_{FSS}\cos^2\theta_i = 0 \tag{6}$$

It could be observed from Equations (4) and (6) that when the incidence angle changed, reflections from the FSS also drastically varied for both TE and TM polarizations. Since reflections from the FSS increased with an increase in incidence angle, the RCS of the MIMO antenna backed by the FSS also increased. To make the RCS of the MIMO antenna insensitive as a function of incidence angle for both the polarizations, an angularly stable FSS needed to be designed.

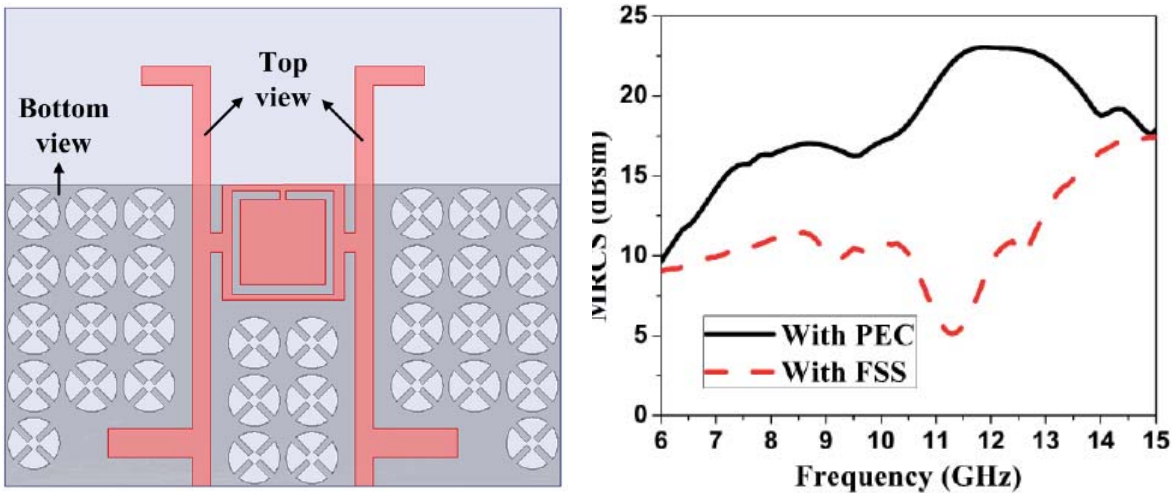

Figure 14. The final proposed low-RCS MIMO antenna: (a) design and (b) simulated monostatic RCS.

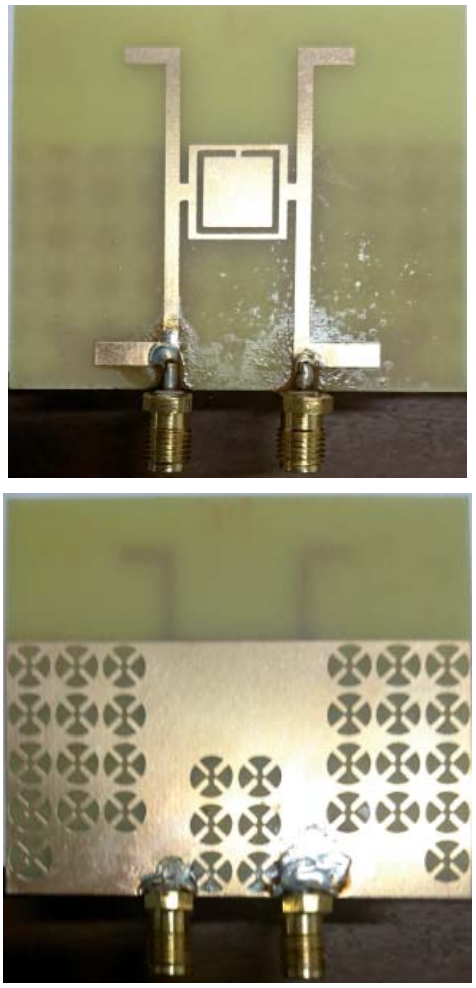

Figure 15. Fabricated (a) top and (b) bottom portions of the proposed low-RCS MIMO antenna.

In Figure 13, a polarization and incidence-angle-insensitive FSS is shown. The four-fold symmetry of the FSS contributed to polarization-angle insensitivity, and the four circular sectors present in the FSS contributed to incidence-angle insensitivity. The designed angularly stable FSS was denoted FSS_2. In Figure 14a, FSS_2 was incorporated into the ground plane of the MIMO antenna. At 11.3 GHz, FSS_2 exhibited bandpass characteristics, as shown in Figure 13b. At the same 11.3 GHz, the maximum RCS reduction was hence achieved by the proposed antenna as compared to the reference antenna, as shown in Figure 14b. With FSS_2, the reduction in RCS was achieved from 6 GHz to 15 GHz with a maximum value of more than 15 dB at 11.3 GHz. The top and bottom views of the final fabricated low-RCS MIMO antenna (i.e., the MIMO antenna with FSS_2) are shown in Figures 15a and 15b, respectively. In Figures 16a-16c, the reflection and transmission properties of FSS_2 are shown when it was under different polarizations and incidence angles. For all the polarization angles, FSS_2 provided a stable response as shown in Figure 16a. Up to incidence angles of 60°, the reflection and transmission properties of FSS_2 remained stable for both polarizations, as shown in Figures 16b and 16c.

It could also be observed from Figures 16b and 16c that the transmission and reflection properties of FSS_2 at different incidence angles were not affected by a change in polarization from TM to TE. The RCS of the MIMO antenna

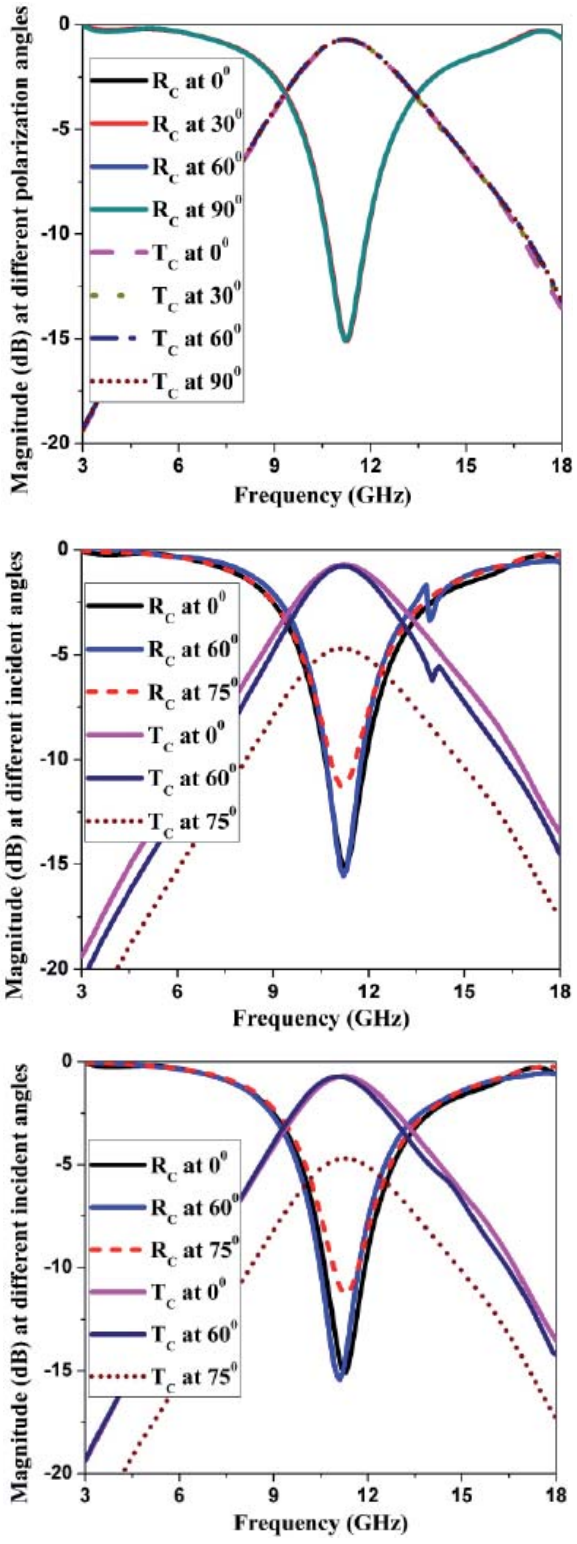

Figure 16. The simulated T_C and R_C of FSS_2 at different (a) polarization angles and (b) incidence angles for a TE plane wave, (c) and incident angles for a TM plane wave.

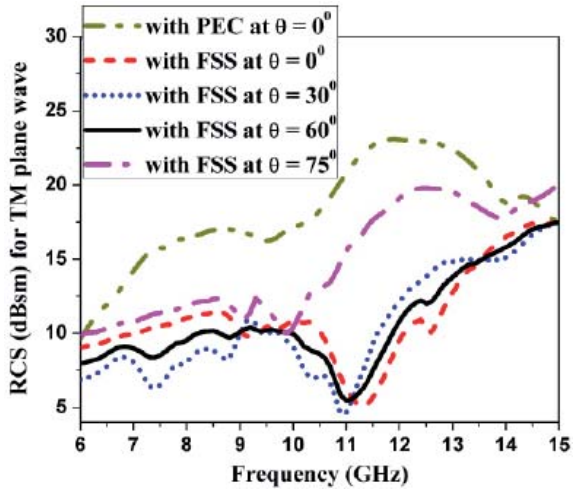

Figure 17. The RCS of the MIMO antenna with FSS_2 at various oblique incidence angles under TM polarization.

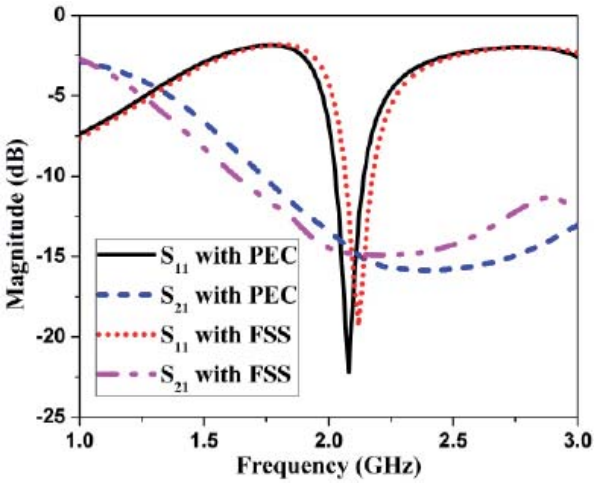

Figure 18. A comparison of measured *S* parameters of the MIMO antenna when backed by PEC and FSS_2.

with FSS_2 at various oblique incidence angles hence also remained unchanged with a change in polarization from TM to TE. Because of this, we measured the RCS of the MIMO antenna with FSS_2 only for TM polarization. The measured RCS results are shown in Figure 17. The same results were also valid for TE polarization, except for small variations that were due to the upper conductive microstrip part. Up to incidence angles of 60°, an almost constant RCS reduction was achieved by the proposed antenna as compared to the reference antenna, as shown in Figure 17. The simulated *S* parameters were validated by measuring them, as shown in Figure 18. With the proposed technique, the reduction in RCS was achieved while preserving the antenna's characteristics. This statement can be verified using Figure 19, in which the measured radiation patterns of MIMO antennas backed by both PEC and FSS_2 are shown. In both the *xz* and *yz* planes, the radiation patterns of the final low-RCS MIMO antenna perfectly matched with the MIMO antenna backed by the PEC. By just replacing the PEC with the angularly stable FSS, the proposed MIMO antenna with a filter-based decoupling network has achieved great practical usefulness.

4. Conclusion

In this paper, a technique for achieving RCS reduction for a two-port MIMO antenna has been presented. Before directly moving into the RCS reduction process, a filter-based decoupled network was designed to improve the isolation among the antenna ports in the MIMO system. Since the decoupling technique presented in this paper is a generalized technique, it can be easily applied to multi-band multi-port MIMO antennas; however, in that case, a multi-frequency band-stop filter would be required. By accommodating an FSS in the ground plane of a MIMO antenna, a reduction in RCS was achieved from 6 GHz to 15 GHz. Unlike previously published RCS reduction techniques, this paper achieved a constant RCS reduction for incidence angles of up to 60°.

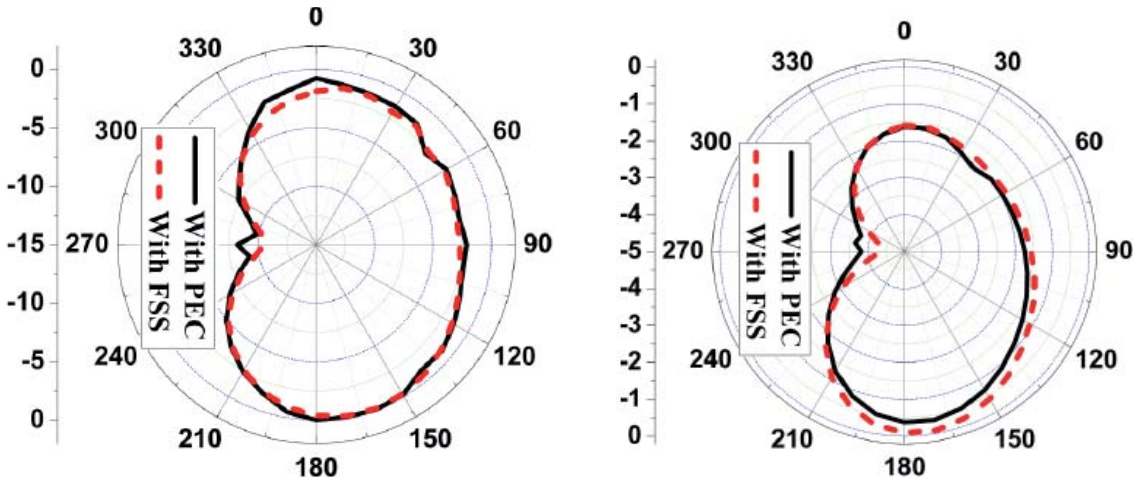

Figure 19. A comparison of the radiation patterns of the MIMO antenna when backed by PEC and FSS_2 in (a) the *xz* plane and the (b) *yz* plane (measured results).

5. References

1. "Mobile Networked Multiple-Input, Multiple-Output (MNM) Program," Arlington, VA, USA, February 2004, Defense Advanced Research Projects Agency, available at: http://www.iwar.org.uk/newsarchive/2004/pdf/darpa-mnm-release2.pdf.

2. R. Boland, "Antenna Experiments Yield Military Benefits," *SIGNAL Magazine*, December, 2012, available at: https://www.afcea.org/content/?q=node/10369/

3. Y. Q. Li, H. Zhang, Y. Q. Fu, and N. C. Yuan, "RCS Reduction of Ridged Waveguide Slot Antenna Array Using EBG Radar Absorbing Material," *IEEE Antennas and Wireless Propagation Letters*, **7**, June 2008, pp. 473-476.

4. H. B. Baskey, E. Johari, and M. J. Akhtar, "Metamaterial Structure Integrated with a Dielectric Absorber for Wideband Reduction of Antennas Radar Cross Section," *IEEE Transactions on Electromagnetic Compatibility*, **59**, 4, August 2017, pp. 1-10.

5. J. L. Volakis, A. Alexanian, and J. M. Lin, "Broadband RCS Reduction of Rectangular Patch by Using Distributed Loading," *Electronics Letters*, **28**, 25, December 1992, pp. 2322-2323.

6. S. Genovesi, F. Costa, and A. Monorchio, "Low-Profile Array with Reduced Radar Cross Section by Using Hybrid Frequency Selective Surfaces," *IEEE Transactions on Antennas and Propagation*, **60**, 5, May 2012, pp. 2327-2335.

7. S. R. Thummaluru, R. Kumar, and R. K. Chaudhary, "Isolation Enhancement and Radar Cross Section Reduction of MIMO Antenna with Frequency Selective Surface," *IEEE Transactions on Antennas and Propagation*, **66**, 3, March 2018, pp. 1595-1600.

8. X. Kang, J. Su, H. Zhang, Z. Li, and Y. Yang, "Ultra-Wideband RCS Reduction of Microstrip Antenna Array by Optimized Multi-Element Metasurface," *Electronics Letters*, **53**, 8, April 2017, pp. 520-522.

9. Y. Liu, K. Li, Y. Jia, Y. Hao, S. Gong, and Y. J. Guo, "Wideband RCS Reduction of a Slot Array Antenna Using Polarization Conversion Metasurfaces," *IEEE Transactions on Antennas and Propagation*, **64**, 1, January 2016, pp. 326-331.

10. M. Mighani, and G. Dadashzadeh, "Broadband RCS Reduction Using a Novel Double Layer Chessboard AMC Surface," *Electronics Letters*, **52**, 14, July 2016, pp. 1253-1255.

11. Y. Wang and Z. Du, "A Wideband Printed Dual-Antenna with Three Neutralization Lines for Mobile Terminals," *IEEE Transactions on Antennas and Propagation*, **62**, 3, March 2014, pp. 1495-1500.

12. R. Anitha, V. P. Sarin, P. Mohanan, and K. Vasudevan, "Enhanced Isolation with Defected Ground Structure in MIMO Antenna," *Electronics Letters*, **50**, 24, November 2014, pp. 1784-1786.

13. C. M. Luo, J. S. Hong, and L. L. Zhong, "Isolation Enhancement of a Very Compact UWB-MIMO Slot Antenna with Two Defected Ground Structures," *IEEE Antennas and Wireless Propagation Letters*, **14**, April 2015, pp. 1766-1769.

14. H. Lee, and B. Lee, "Compact Broadband Dual-Polarized for Indoor MIMO Wireless Communication Systems," *IEEE Transactions on Antennas and Propagation*, **64**, 2, February 2016, pp. 766-770.

15. Z. Li, Z. Du, M. Takahashi, K. Saito, and K. Ito, "Reducing Mutual Coupling of MIMO Antennas with Parasitic Elements for Mobile Terminals," *IEEE Transactions on Antennas and Propagation*, **60**, 2, February 2012, pp. 473-481.

16. S. W. Su, C. T. Lee, and F. S. Chang, "Printed MIMO-Antenna Systems Using Neutralization-Line Technique for Wireless USB-Dongle Applications," *IEEE Transactions on Antennas and Propagation*, **60**,2, February 2012, pp. 456-463.

17. S. Zhang, G. F. Pedersen, "Mutual Coupling Reduction for UWB MIMO Antennas with a Wideband Neutralization Line," *IEEE Antennas Wireless Propagation Letters*, **15**, May 2016, pp. 166–169.

18. C.-H. Wu, C.-L. Chiu, and T.-G. Ma, "Very Compact Fully Lumped Decoupling Network for a Coupled Two-Element Array," *IEEE Antennas and Wireless Propagation Letters*, **15**, May 2015, pp. 158-161.

19. S. C. Chen, Y. S. Wang, and S. J. Chung, "A Decoupling Technique for Increasing the Port Isolation Between Two Strongly Coupled Antennas," *IEEE Transactions on Antennas and Propagation*, **56**, 12, December 2008, pp. 3650-3658.

20. M. M. Bait-Suwailam, M. S. Boybay, and O. M. Ramahi, "Electromagnetic Coupling Reduction in High-Profile Monopole Antennas Using Single-Negative Magnetic Metamaterials for MIMO Applications," *IEEE Transactions on Antennas and Propagation*, **58**, 9, September 2010, pp. 2894-2902.

21. G. Zhai, Z. N. Chen, and X. Qing, "Enhanced Isolation of a Closely Spaced Four-Element MIMO Antenna System Using Metamaterial Mushroom," *IEEE Transactions on Antennas and Propagation*, **63**, 8, August 2015, pp. 3362-3370.

22. C. X. Mao, and Q. X. Chu, "Compact Co-Radiator UWB-MIMO Antenna with Dual Polarization," *IEEE Transactions on Antennas and Propagation*, **62**, 9, September 2014, pp. 4474-4480.

23. Y. K. Choukiker, S. K. Sharma, and S. K. Behera, "Hybrid Fractal Shape Planar Monopole Antenna Covering Multiband Wireless Communications with MIMO Implementation for Handheld Mobile Devices," *IEEE Transactions on Antennas and Propagation*, **62**, 3, March 2014, pp. 1483-1488.